RSC Advances

PAPER

View Article Online
View Journal | View Issue

Cite this: *RSC Adv.*, 2025, **15**, 28137

Differential changes of trichloroethylene degradation efficiency and carbon isotope fractionation during oxygenation of different Fe(II) species

Rong Chen, *[a] Jiayu Liu*[b] and Hao Yu[c]

Hydroxyl radicals (˙OH) generated from Fe(II) oxidation by O_2 play a key role in chlorinated hydrocarbon (CHC) degradation, yet the effects of different Fe(II) species on degradation kinetics and carbon isotope fractionation remain unclear. Using trichloroethylene (TCE) as a model CHC, this study demonstrates that Fe(II) species influence TCE degradation *via* variations in ˙OH production rates, efficiencies, and quenching capacities. After 24 h, TCE degradation efficiencies followed the order: Fe(II) in rNAu-2 (72.4%) > Fe(II)-citrate (52.6%) > $FeCO_3$ (46.1%) > Fe(II)–Al_2O_3 (27.6%) > dissolved Fe(II) (7.9%). This outcome can be attributed to two aspects: (1) the rate and efficiency of ˙OH production were highest for Fe(II)-citrate, moderate for Fe(II) adsorbed on Al_2O_3 and mineral structural Fe(II), and lowest for inorganic $Fe(II)_{dis}$. (2) Fe(II)-citrate had the highest quenching efficiency, followed by inorganic $Fe(II)_{dis}$ and adsorbed Fe(II), with mineral structural Fe(II) being lowest. Despite these differences, carbon isotope enrichment factors ($\varepsilon^{13}C$) were relatively consistent across systems (average $\varepsilon^{13}C = -1.6‰ \pm 0.6‰$), distinct from most other reported degradation mechanisms. These results advance our understanding of ˙OH-mediated TCE degradation and aid in differentiating ˙OH pathways from other natural attenuation processes.

Received 29th November 2024
Accepted 9th July 2025

DOI: 10.1039/d4ra08439j

rsc.li/rsc-advances

1. Introduction

Chlorinated hydrocarbons (CHCs), extensively used in industry, have become widespread soil and groundwater contaminants due to improper disposal.[1] Their subsurface fate and transport have garnered significant attention,[2,3] with natural attenuation shown to depend heavily on redox conditions.[4] Under anoxic conditions, reductive dechlorination by specific microbes and reductants predominates,[5] whereas aerobic biological oxidation dominates under oxic conditions.[3] Recent findings reveal that hydroxyl radical (˙OH)-mediated abiotic oxidation also plays a major role under fluctuating redox conditions, proceeding at rates several orders of magnitude higher than reductive pathways systems.[4,6] Given the critical role of ˙OH oxidation in CHC attenuation, it is essential to investigate various aspects of CHC degradation and ˙OH production in subsurface environments.

Abiotic reduction of O_2 by Fe(II) is the primary source of ˙OH in organic carbon-poor subsurface environments.[7–9] This process, described by the Haber–Weiss mechanism.[10] According to eqn (1)–(4), the oxidation of Fe(II) by O_2 is the rate-limited step and the decomposition of H_2O_2 by Fe(II) governs ˙OH production. Both the rate constant of Fe(II) and ˙OH yield are strongly dependent on Fe(II) reactivity,[11,12] leading to significant variability among Fe(II) species. In CHC degradation, Fe(II) contributes to ˙OH generation but may also act as a sink by competitively quenching ˙OH (eqn (4)). In general, the quenching effect of Fe(II) is related to both Fe(II) species and concentrations.[12] Thus, Fe(II) species can play dual or multiple roles in CHC transformation during oxygenation.

$$Fe(II) + O_2 \rightarrow Fe(III) + {}^{\cdot}O_2^- \quad (1)$$

$$Fe(II) + {}^{\cdot}O_2^- + 2H^+ \rightarrow Fe(III) + H_2O_2 \quad (2)$$

$$Fe(II) + H_2O_2 \rightarrow Fe(III) + {}^{\cdot}OH + OH^- \quad (3)$$

$$Fe(II) + {}^{\cdot}OH \rightarrow Fe(III) + OH^- \quad (4)$$

Oxidation of trichloroethene (TCE), a representative CHC, has been reported in sediment system.[4,12] However, notable differences in ˙OH production and TCE degradation have been observed across different sediment systems, presumably due to differences in Fe(II) species.[11,12] Xie *et al.* demonstrated that

[a]*School of Environmental and Biological Engineering, Wuhan Technology and Business University, 3 Huangjiahu West Road, Wuhan 430065, P. R. China. E-mail: chenrong@cug.edu.cn*

[b]*Middle Changjiang River Bureau of Hydrology and Water Resources Survey, Bureau of Hydrology, Water Resources Commission, Wuhan 430012, P. R. China. E-mail: 1552152510@qq.com*

[c]*Applied Technology Innovation Center of Rare Earth Resources, China Geological Survey, No. 5, South Section 3, Second Ring Road, Chengdu, Sichuan, 610041, P. R. China*

ligand-mediated regulation of Fe(II) speciation enhances TCE degradation in sediments.[13] However, due to sediment heterogeneity, the specific roles of different Fe(II) species remain unclear. While prior studies have examined Fe-bearing clay minerals and pyrite,[6,14] the effects of other Fe(II) species including inorganic dissolved Fe(II), complexed Fe(II), mineral adsorbed Fe(II) and ferrous carbonate on TCE degradation, remain unexplored.

While TCE degradation during Fe(II) oxygenation has been studied, carbon isotope fractionation of TCE remains unexplored. Compound-specific isotope analysis (CSIA) is a powerful tool for assessing contaminant degradation and elucidating mechanisms at field scale.[15–17] Given that isotope fractionation is governed by reaction mechanisms,[4,18,19] CSIA may help identify $^{\bullet}$OH oxidation and quantify TCE removal. However, the carbon isotope fractionation of TCE by $^{\bullet}$OH oxidation during the oxygenation of Fe(II) species and the influence of Fe(II) species remains unclear. If Fe(II) species exert limited influence on this fractionation, CSIA could serve as a key indicator of $^{\bullet}$OH involvement and its contribution to TCE degradation in natural systems.

This study aimed to assess the effects of various Fe(II) species on TCE degradation and quantify the carbon isotope enrichment factor (ε) during Fe(II) oxygenation. Representative species included dissolved, complexed, and surface-adsorbed Fe(II), as well as $FeCO_3$ and nontronite (NAu-2). $^{\bullet}$OH production was evaluated *via* benzoate oxidation to *p*-hydroxybenzoic acid.[20] Batch experiments examined TCE degradation, $^{\bullet}$OH generation, and associated carbon isotope fractionation, contributing to a better understanding of TCE transformation at anoxic–oxic interfaces.

2. Materials and methods

2.1. Chemicals and materials

Ferrous sulfate heptahydrate ($FeSO_4 \cdot 7H_2O$, 99%), sodium benzoate (99.5%), *p*-hydroxybenzoic acid (*p*-HBA, 99%), sodium carbonate (Na_2CO_3, 99.9%), mercuric chloride ($HgCl_2$, 99.5%), and Al_2O_3 (>98%) were purchased from Sinopharm Chemical Reagent Co., Ltd, China. TCE was acquired from J&K Scientific. All other chemicals were of analytical grade or higher. Deionized (DI) water, with a resistance of 18.2 MΩ cm obtained from a Heal Force NW ultrapure water system, was utilized for all experiments. A saturated solution of TCE (1075 mg L^{-1}) was prepared by adding excess TCE to DI water.

Inorganic dissolved Fe(II), complexed Fe(II), surface adsorbed Fe(II), $FeCO_3$ and reduced NAu-2 (rNAu-2) were prepared by the following procedures. It is noted that to prepare the O_2-free water, DI water was purged with high purity N_2 (99.999%) for 2 h to remove residual O_2. Inorganic dissolved Fe(II) ($Fe(II)_{dis}$) was prepared by dissolving $FeSO_4$ in O_2-free solution within a pH of 2–3. Complexed Fe(II) was obtained by complexing $Fe(II)_{dis}$ and citrate in a 1 : 1 molar ratio at pH 6 (Fe(II)-citrate). Surface adsorbed Fe(II) was produced by adsorbing of $Fe(II)_{dis}$ onto Al_2O_3 (Fe(II) adsorbed on Al_2O_3). Specifically, 10 mM $Fe(II)_{dis}$ was mixed with 100 g per L Al_2O_3 for 4 h under anoxic conditions.[11] Approximately 98% $Fe(II)_{dis}$ was adsorbed on Al_2O_3, as the residual dissolved Fe(II) ($Fe(II)_{dis}$) concentration was less than 0.2 mM. $FeCO_3$ was synthesized *via* the precipitation of $Fe(II)_{dis}$ and Na_2CO_3.[21] In detail, equal volumes of 0.5 M $FeSO_4$ and 0.5 M Na_2CO_3 was mixed and reacted in an anaerobic glovebox (COY, USA) for 12 h. The resulting solid suspension was $FeCO_3$. NAu-2 (23% Fe content by weight) was sourced from the Clay Minerals Society's Source Clays Repository (West Lafayette, Indiana). Since the purchased NAu-2 was in an oxidized state, it was reduced using a modified dithionite-citrate-bicarbonate (DCB) method.[22] The fraction of Fe(II) in total Fe in the reduced NAu-2 (rNAu-2) was measured to be 48.2% based on a modified chemical extraction method.[23] The specific surface areas of Al_2O_3, $FeCO_3$, and rNAu-2 were measured as 164.2, 32.9, and 13.2 $m^2\ g^{-1}$, respectively.

2.2. Oxygenation experiments

All experiments were conducted in 121 mL bottles at 25 °C. To prevent photochemical interference, each bottle was wrapped with tin foil. In a typical experiment, a certain volume of Fe(II) suspension was firstly mixed with 80 mL of O_2-free water, and then 0.075 mL of TCE-saturated solution was added to achieve an initial concentration of 7.6 μM (*i.e.*, ~1 mg L^{-1}). The bottle was immediately sealed with a thick butyl rubber stopper and an aluminum foil cap. The concentration of Fe(II) is a critical parameter for $^{\bullet}$;OH production and TCE degradation, with previously reported ranges spanning from several mM to hundreds of mM.[13,24,25] Preliminary experiments showed that Fe(II) concentration at 10 mM achieve the effective degradation of TCE. Hence, the initial Fe(II) concentrations in the systems of inorganic $Fe(II)_{dis}$, Fe(II)-citrate, Fe(II) adsorbed on Al_2O_3, $FeCO_3$, and rNAu-2 systems were set to 10 mM. To initiate the experiment, 15 mL of O_2 (80%) was injected into the reactor to ensure sufficient O_2 levels (see Section S1). The solution pH was manually adjusted to 6 by adding H_2SO_4 and NaOH during the reaction course, and the pH variation was less than 0.2 units throughout the experiment. The reactor was placed on a vibrating cultivation box set at a constant speed of 220 rpm. Control experiments with the addition of 1 M 2-propanol and 0.1% $HgCl_2$ were conducted to quench $^{\bullet}$;OH oxidation and inhibit microbial activity, respectively.

To investigate $^{\bullet}$;OH production during oxygenation, 20 mM benzoate was added instead of 7.6 μM TCE to the Fe(II) suspension, with all other experimental conditions unchanged. At predetermined time intervals (0–24 h), approximately 3 mL samples were collected to analyze TCE concentration and its carbon isotope composition ($\delta^{13}C$), *p*-HBA, and Fe(II). All experiments were performed in at least duplicate. In all figures, points, and error bars represent the averaged values and standard deviations for the duplicate experiments.

2.3. Chemical analysis

For the analysis of TCE concentration, 1 mL solution sample mixed with 2 mL of hexane and shaken for at least for 0.5 h to ensure complete extraction of TCE from aqueous phase into hexane phase. Subsequently, the concentration of TCE in hexane was measured using a gas chromatograph (GC,

Shimadzu 2014C, Japan) equipped with an electron capture detector (ECD) and a capillary column. The column temperature was maintained at 55 °C, while the injector and detector temperatures were set at 230 and 280 °C, respectively. The concentration of *p*-HBA was measured using a high-performance liquid chromatograph (HPLC, Shimadzu LC-15C, Japan) equipped with a UV detector and an Inter Sustain C18 column.[20] Fe(II) concentration was assessed by the 1, 10-*o*-phenanthrolin method at 510 nm using a UV-vis spectrophotometer.[23]

For $\delta^{13}C$ analysis of TCE, 1 mL of sample was mixed with 1 mL of 2 M NaCl solution and stored at −20 °C. Before analysis, the samples were thawed. Preliminary experiments indicated that these treatments minimized the volatilization of TCE and had a negligible influence on $\delta^{13}C$ values. The $\delta^{13}C$ of TCE was determined using a gas chromatography-combustion-isotope ratio mass spectrometer (GC-C-IRMS, MAT253), as previously described.[26] Briefly, TCE in solution was extracted using a solid-phase microextraction fiber (SPME) coated with 100 μm polydimethylsiloxane (Supelco, Bellefonte, PA, USA) in the headspace. The SPME fiber was then inserted into the GC injector (230 °C) to thermally desorb the TCE. The $\delta^{13}C$ values were reported relative to a CO_2 reference gas, with an accuracy of 0.5‰.[19]

2.4. Kinetic analysis

Previous studies have shown that the oxidation of inorganic dissolved Fe(II) by O_2 can be described using a pseudo-first-order kinetic model.[27] In this study, the Fe(II) oxidation by O_2 reached steady state within 24 h, so the pseudo-first-order kinetic equation was modified as follow:

$$[Fe(II)]_t = ([Fe(II)]_0 - [Fe(II)]_{unreacted}) \exp(-k_{app}t) + [Fe(II)]_{unreacted} \quad (5)$$

where $[Fe(II)]_t$ represents the concentration of residual total Fe(II) at time t during the reaction; $[Fe(II)]_0$ represent the initial concentrations of total Fe(II); $[Fe(II)]_{unreacted}$ represents the concentration of unoxidized Fe(II); k_{app} represents the apparent rate constant.

3. Results and discussion

3.1. Effect of Fe(II) species on ·OH production during oxygenation

Prior to exploring TCE degradation, the influence of Fe(II) species on ·OH production was examined. The results showed that ·OH was produced during the oxygenation of Fe(II) species (Fig. 1), aligning with previous findings that Fe(II) oxidation can couple with the generation of ·OH from O_2 reduction.[6,7,28,29] For oxygenation of 10 mM Fe(II), the ·OH accumulations over 24 h for inorganic $Fe(II)_{dis}$, Fe(II)-citrate, Fe(II) adsorbed on Al_2O_3, $FeCO_3$, and Fe(II) in rNAu-2 systems were 16.3, 487.5, 100.4, 31.6 and 218.2 μM, respectively (Fig. 1a). The oxidation of Fe(II) followed a pseudo-first-order kinetic model in most cases, with rate constants of 0.02, 0.14, 0.58, 0.13 and 0.37 h^{-1} for inorganic $Fe(II)_{dis}$, Fe(II)-citrate, Fe(II) adsorbed on Al_2O_3, $FeCO_3$, and Fe(II)

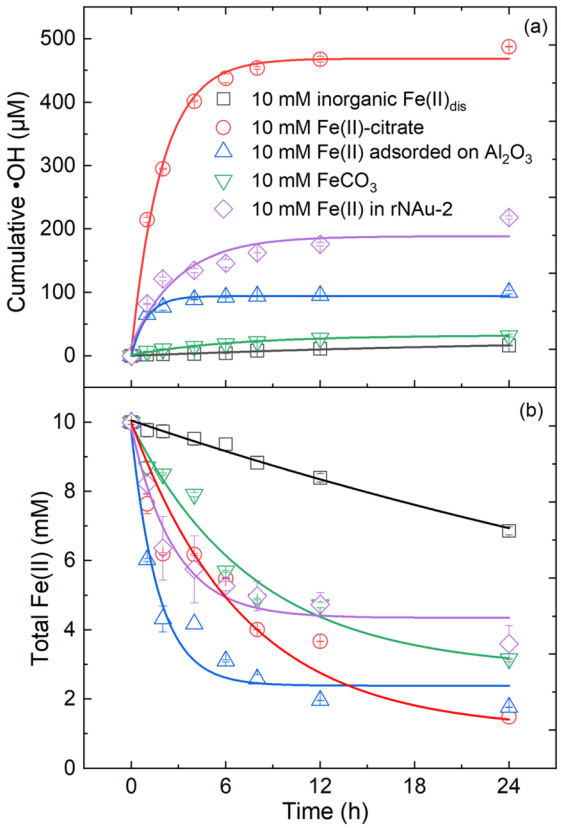

Fig. 1 (a) ·OH production and (b) Fe(II) oxidation during the oxygenation of Fe(II) species. Initial reaction conditions: 10 mM Fe(II), pH 6.0 and oxic conditions, unless otherwise specified.

in rNAu-2, respectively (Fig. 1b and Table S1). These results suggest that the reactivity of different Fe(II) species toward O_2 followed the order: Fe(II) adsorbed on Al_2O_3 > Fe(II) in rNAu-2 > Fe(II)-citrate > $FeCO_3$ > inorganic $Fe(II)_{dis}$.

To explore the relationship between Fe(II) species and ·OH production, the electron utilization efficiency (EUE) of Fe(II) oxidation was calculated based on eqn (5). Correction analysis showed that the EUE values for inorganic $Fe(II)_{dis}$, Fe(II)-citrate, Fe(II) adsorbed on Al_2O_3, $FeCO_3$, and Fe(II) in rNAu-2 were 1.7%, 22%, 3.9%, 1.4%, and 9.9%, respectively (Fig. S1 and Table 1). These results indicate that the EUE for ·OH production followed the orders: Fe(II)-citrate > Fe(II) in rNAu-2 > Fe(II) adsorbed on Al_2O_3 > inorganic $Fe(II)_{dis}$ > $FeCO_3$, which is roughly opposite of the reactivity of Fe(II) toward O_2. That is, the higher reactivity of Fe(II) correlated with the lower efficiency in the catalytic decomposition of H_2O_2 to produce ·OH. This trend can be explained by the fact that the decomposition of H_2O_2 is a crucial step in ·OH production during the oxygenation of Fe(II) (eqn (6)), while the yield of ·OH from H_2O_2 decomposition decreased with increasing Fe(II) reactivity.[11,30]

$$EUE = \frac{3 \times c_{\cdot OH}}{c_{0,Fe(II)} - c_{t,Fe(II)}} \times 100\% \quad (6)$$

where EUE represents the electron utilization efficiency for ·OH production from Fe(II) oxidation; $c_{\cdot OH}$ represents the ·OH accumulation during oxygenation; $c_{0,\ Fe(II)}$ and $c_{t,\ F(II)}$ represent

Table 1 A summary of ˙OH yield, residual Fe(II), electron utilization efficiency of Fe(II), ˙OH utilization efficiency and carbon isotope enrichment coefficient in different Fe(II) system

Fe(II) species	˙OH yield (μM)	Residual Fe(II) (mM)	EUE (%)	˙OH utilization efficiency (%)	$\varepsilon^{13}C$ (‰)
Inorganic $Fe(II)_{dis}$	16.3 ± 0.5	6.9 ± 0.1	1.7 ± 0.1	3.4 ± 0.2	—
Fe(II)-citrate	487.5 ± 0.7	1.5 ± 0.01	22 ± 1.8	0.8 ± 0.03	−1.5 ± 0.3
Fe(II) adsorbed on Al_2O_3	100.4 ± 2.8	1.8 ± 0.01	3.9 ± 0.2	1.3 ± 0.2	−0.9 ± 0.2
$FeCO_3$	31.6 ± 2.3	3.2 ± 0.02	1.4 ± 0.1	13 ± 0.9	−2.1 ± 0.2
Fe(II) in rNAu-2	218.2 ± 2.6	3.6 ± 0.5	9.9 ± 0.3	3.2 ± 0.2	−2 ± 0.4

the initial and instantaneous concentrations of Fe(II), respectively.

3.2. Effect of Fe(II) species on TCE degradation during oxygenation

Control experiments showed that the variation of TCE in aqueous solution was less than 2% and the addition of 0.1% $HgCl_2$ had had minimal impact on TCE degradation (Fig. S2), suggesting that volatilization and microbial oxidation played a negligible role in TCE degradation. However, when 1 M 2-propanol was added, the degradation of TCE became negligible (Fig. S2). As 2-propanol is an ˙OH scavenger,[20] this notable quenching effect indicates that ˙OH primarily contributed to TCE degradation.

After 24 hours of oxygenation, TCE concentration decreased from 7.6 to 7, 3.6, 5.5, 4.1, and 2.1 μM in the inorganic $Fe(II)_{dis}$, Fe(II)-citrate, Fe(II) adsorbed on Al_2O_3, $FeCO_3$, and Fe(II) in rNAu-2 systems, respectively (Fig. 2a). Thus, the degradation efficiencies of TCE were estimated to be 7.9%, 52.6%, 27.6%, 46.1%, and 72.4% in these above Fe(II) systems, respectively (Fig. 2a). Consequently, the dependence of TCE degradation on different Fe(II) species followed the sequence: Fe(II) in rNAu-2 > Fe(II)-citrate > $FeCO_3$ > Fe(II) adsorbed on Al_2O_3 > inorganic $Fe(II)_{dis}$. Notably, this sequence did not correspond to ˙OH yield produced by different Fe(II) species. The removal efficiency of TCE (RET) was calculated based on eqn (7).

$$\mathrm{RET} = \frac{c_{0,\mathrm{TCE}} - c_{t,\mathrm{TCE}}}{c_{0,\mathrm{TCE}}} \times 100\% \quad (7)$$

where $c_{0,\ \mathrm{TCE}}$ and $c_{t,\ \mathrm{TCE}}$ represent the initial and instantaneous concentrations of TCE, respectively.

To further understand the influence of Fe(II) species on TCE degradation *via* ˙OH oxidation, the ˙OH utilization efficiency in different Fe(II) system was estimated. Linear correlation analysis between TCE reduction and ˙OH accumulation showed that the ˙OH utilization efficiencies were 3.4%, 0.8%, 1.3%, 13%, and 3.2% for inorganic $Fe(II)_{dis}$, Fe(II)-citrate, Fe(II) adsorbed on Al_2O_3, $FeCO_3$, and Fe(II) in rNAu-2 systems, respectively (Fig. 2b and Table 1). The variation in ˙OH utilization efficiency among Fe(II) systems may be attributed to the quenching effects of Fe(II) and other reduced species. The quenching efficiency (QE) of co-existing compounds on TCE ($k_{\mathrm{TCE},\ \cdot\mathrm{OH}} = 4.2 \times 10^9\ \mathrm{M^{-1}\ s^{-1}}$)[13] degradation was calculated using eqn (8).

$$\mathrm{QE} = \frac{\sum c_i k_{i,\cdot\mathrm{OH}}}{\sum c_i k_{i,\cdot\mathrm{OH}} + c_{\mathrm{TCE}} k_{\mathrm{TCE},\cdot\mathrm{OH}}} \times 100\% \quad (8)$$

where c_i and c_{TCE} denote the concentrations of co-existing components and TCE, respectively; $k_{i,\ \cdot\mathrm{OH}}$ and $k_{\mathrm{TCE},\ \cdot\mathrm{OH}}$ represent the rate constants for the reaction of ˙OH with co-existing components and TCE, respectively.

After 24 h of oxygenation, the residual Fe(II) concentrations were 5.5, 1.5, 1.8, 3.2, and 3.6 mM in the inorganic $Fe(II)_{dis}$, Fe(II)-citrate, Fe(II) adsorbed on Al_2O_3, $FeCO_3$, and Fe(II) in rNAu-2 systems, respectively (Fig. 1b). As the rate constant of Fe(II) oxidation by ˙OH was 1×10^8–$3.5 \times 10^8\ \mathrm{M^{-1}\ s^{-1}}$,[12,25] the quenching efficiencies of the residual Fe(II) on TCE degradation

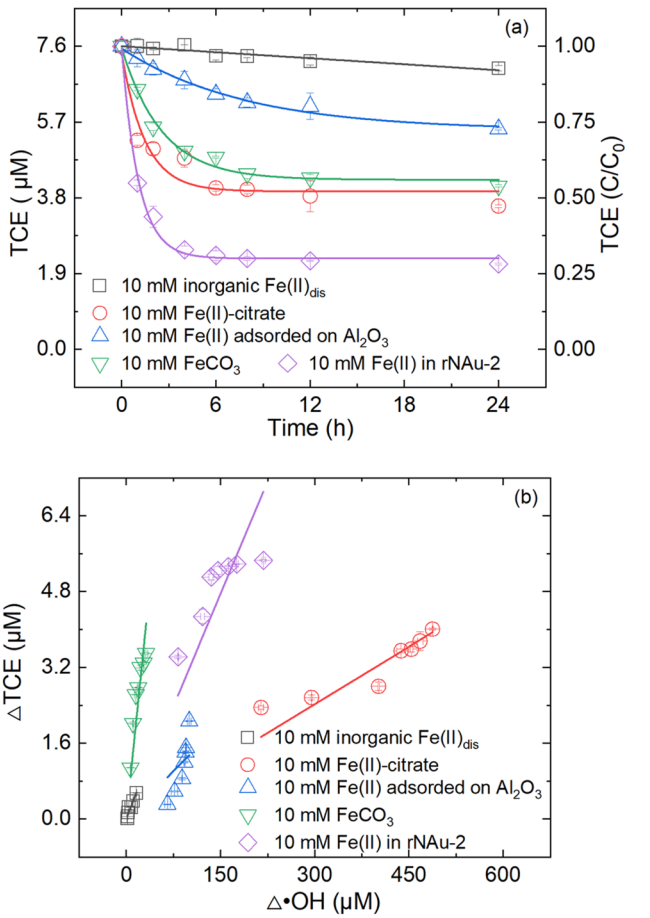

Fig. 2 (a) Variation of TCE concentration during oxygenation of different Fe(II) species and (b) linear relationship between ˙OH accumulation and TCE degradation. Initial reaction conditions: 10 mM Fe(II), pH 6.0 and under oxic condition.

were estimated to be ~98.3%, ~94.3%, 84.9–95.2%, 90.9–97.2%, and 91.9–97.5%, respectively (Section S2). Therefore, the ˙OH utilization efficiencies by TCE in inorganic $Fe(II)_{dis}$, Fe(II)-citrate, Fe(II) adsorbed on Al_2O_3, $FeCO_3$, and Fe(II) in rNAu-2 systems were ~1.7%, ~5.7%, 4.8–15.1%, 2.8–9.1%, and 2.5–8.1%, respectively. The calculated ˙OH utilization efficiencies for the inorganic $Fe(II)_{dis}$, $FeCO_3$, and Fe(II) in rNAu-2 systems were consistent with the measured values (Table 1). However, in the Fe(II)-citrate and Fe(II) adsorbed on Al_2O_3 systems, the calculated ˙OH utilization efficiencies were overestimated (Table 1). This suggests that in these systems, other reduced species may compete with TCE for ˙OH consumption. In the Fe(II)-citrate system, when Fe(II)-citrate was oxidized to Fe(III)-citrate, the Fe(III)-citrate can also react with ˙OH, with the rate constant of 1.2×10^8 M^{-1} s^{-1}.[31] In the Fe(II)–Al_2O_3 system, the surface –OH groups of Al_2O_3 may quench ˙OH.[32] Therefore, in both Fe(III)-citrate and Fe(II)–Al_2O_3 systems, in addition to Fe(II), competition for ˙OH from the ligand and the adsorbent notably decreased ˙OH utilization efficiency.

In summary, the influence of Fe(II) species on TCE degradation can be attributed to the following aspects: the rate and efficiency of ˙OH production, as well as the quenching effect. For ˙OH production, ligand-complexed Fe(II) exhibited the highest rate and efficiency, followed by adsorbed Fe(II) and mineral structural Fe(II), with inorganic $Fe(II)_{dis}$ being lowest. In terms of the quenching effect, ligand-complexed Fe(II) had the highest quenching efficiency, followed by inorganic $Fe(II)_{dis}$ and adsorbed Fe(II), while mineral structural Fe(II) showed the lowest quenching effect.

3.3. Effect of Fe(II) species on carbon isotope fractionation of TCE degradation

To explore the influence of Fe(II) species on carbon isotope fractionation of TCE during oxygenation, the changes in $\delta^{13}C$ values of TCE were measured. During oxygenation, the $\delta^{13}C$ values of TCE gradually increased from −23.8‰ to −22.5‰, −23.3‰, −22.4‰ and −20.6‰ in Fe(II)-citrate, Fe(II) adsorbed on Al_2O_3, $FeCO_3$, and Fe(II) in rNAu-2 systems (Fig. 3). It should be noted that the variation in $\delta^{13}C$ of TCE in the inorganic $Fe(II)_{dis}$ system was negligible (data not shown). Previous studies have demonstrated that chemical bonds with lighter isotopes are weaker than those with heavier isotopes,[15,33,34] so molecules containing heavier isotopes become enriched as degradation progresses. Thus, the increase in $\delta^{13}C$ of residual TCE confirmed that TCE was degraded rather than volatilized during the oxygenation of Fe(II) species. To gain further insight into the carbon isotope fractionation of TCE degradation by ˙OH, the carbon isotope enrichment factor (ε) was calculated according to the Rayleigh equation (eqn (9)).[35]

$$\varepsilon \ln\left(\frac{c}{c_0}\right) = \ln\left(\frac{\delta^{13}C + 1}{\delta^{13}C_0 + 1}\right) \quad (9)$$

where c and c_0 represent the residual and initial concentrations of TCE, respectively; $\delta^{13}C$ and $\delta^{13}C_0$ represent the ^{13}C isotope of the residual and initial TCE.

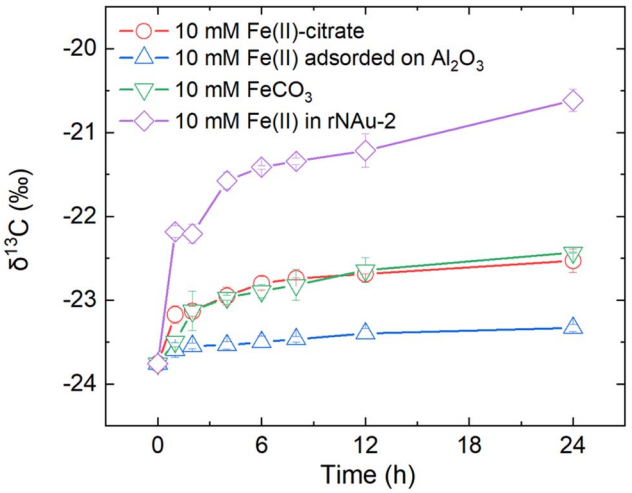

Fig. 3 Variaiton in $\delta^{13}C$ value of residual TCE during oxygenation of different Fe(II) species. Initial reaction conditions: 10 mM Fe(II), pH 6.0 and under oxic condition.

The results showed that the carbon isotope enrichment factors ($\varepsilon^{13}C$) for TCE degradation in the Fe(II)-citrate, Fe(II) adsorbed on Al_2O_3, $FeCO_3$, and rNAu-2 systems were −1.5‰, −0.9‰, −2.1‰, and −2‰, respectively (Fig. 4 and Table 1). The similar $\varepsilon^{13}C$ values in different Fe(II) systems suggest that the influence of Fe(II) species on carbon isotope fractionation during TCE degradation was negligible, giving an averaged carbon isotope enrichment factor of −1.6‰ ± 0.6‰ for TCE degradation by ˙OH. To further verify the independence between carbon isotope enrichment factors and Fe(II) species, carbon isotope fractionation for TCE degradation in sediment system was tested. It is noted that TCE degradation in the sediment system was mainly attributed to ˙OH oxidation (Fig. S2). As shown in Fig. S3, $\varepsilon^{13}C$ for TCE degradation in the sediment system was −1.5‰, which closely matched the

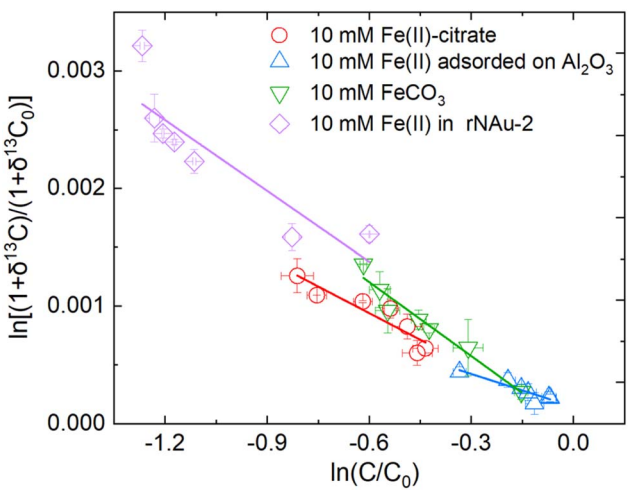

Fig. 4 Rayleigh plots for carbon isotope fractionation during TCE degradation in different Fe(II) systems. Initial conditions: 10 mM Fe(II), pH 6.0 and under oxic condition.

Table 2 Summary of ^{13}C enrichment factors of TCE degradation across different processes

Degradation mechanism	Reaction system	ε (‰)	Source
·OH oxidation	Fe(II)/O_2	−1.6 ± 0.6	This study
Microbial oxidation	*Burkholderiacepacia* G4	−18.2–20.7	38
Microbial oxidation	*Pseudomonas putida* F1	−11.5 ± 2.4	33
Microbial oxidation	*Methylosinus trichosporium* OB3b	−1.1–4.2	33 and 39
Microbial reduction	Multiple *D. mccarty*i strains/*D. mccartyi* 195	−9.6–13.5	40
Abiotic reduction	FeS	−27.9–33.4	41

averaged $\varepsilon^{13}C$ value (−1.6 ± 0.6‰) observed in individual Fe(II) systems. These findings reinforce the conclusion that Fe(II) species have a negligible influence on the carbon isotope enrichment factor for TCE degradation. This independence may be attributed to the dominant role of ·OH oxidation in TCE degradation during the oxygenation of Fe(II) and sediments.

3.4. Comparison with previously reported ^{13}C enrichment factor during TCE degradation

An important goal of carbon isotope analysis of TCE is to identify the degradation pathway of TCE in natural environment. Therefore, we compared the difference in the carbon isotope enrichment factor for TCE degradation *via* ·OH oxidation and other previously reported mechanisms. As shown in Table 2, the carbon isotope enrichment factors for TCE degradation through ·OH oxidation, microbial oxidation, microbial reduction, and abiotic reduction were −1.6 ± 0.6‰, −1.1–20.7‰, −9.6–13.5‰, and −27.9–33.4‰, respectively. These results suggest that the carbon isotope fractionation effect of ·OH oxidation partially overlapped with microbial oxidation pathway, but was significantly different from the microbial and abiotic reduction pathways. However, it is important to note that ·OH oxidation and microbial oxidation occurred in different spatiotemporal scenarios.[36,37] For instance, when reduced sediment is exposed to O_2, ·OH oxidation first contributes to contaminant transformation, after which microbial oxidation becomes the predominant pathway.[36] Additionally, the carbon isotope fractionation effect of ·OH oxidation overlapped with that of microbial oxidation by specific microbe, such as *Methylosinus trichosporium* OB3b (Table 2). As a summary, to distinguish between ·OH oxidation and microbial oxidation, a combination of methods is recommended. This includes carbon isotope analysis, hydrogeological condition monitoring (*e.g.*, groundwater flow, redox conditions, and sediment compositions), and microbial community analysis.

3.5. Environmental implications

TCE degradation *via* ·OH oxidation is considered as an important pathway for the natural attenuation of TCE in the subsurface environments.[4,6,12] However, the identification and quantification of the ·OH oxidation pathway remain a significant challenge. Our findings suggest that carbon isotope fractionation of TCE resulting from ·OH oxidation is independent of Fe(II) species and is significantly different from most other mechanisms. Therefore, carbon isotope analysis could provide valuable guidance for identifying ·OH oxidation pathways.

In terms of contaminant remediation, technologies based on O_2 reduction to produce ·OH have been proposed as environmentally friendly and cost-effective solutions.[42] However, the low electron utilization efficiency of Fe(II) in soils and sediments may constraint the application of this technology.[11] One alternative is to add ligands to convert solid phase Fe(II) into complexed Fe(II), thus improving the electron utilization efficiency of Fe(II) in soils and sediments.[13] However, organic ligands (*e.g.*, citrate) may compete with the target contaminant to consume ·OH. Therefore, when selecting ligands, both the improvement of electron utilization efficiency and the potential quenching effect on ·OH should be considered.

For the degradation of TCE, as Fe(II) species play a critical role in the degradation of TCE, regulating Fe(II) speciation may be a promising strategy to enhance TCE degradation in natural environments. However, the complex chemical constitution of soils/sediments may affect the effectiveness of this enhancement. Consequently, pilot-scale and field-scale tests are needed to evaluate practical applicability. Regarding the carbon isotope fractionation, different reduced species including Fe(II), reduced organic matter and sulfur in sediments/soils may contribute to ·OH production, which subsequently oxidizes TCE during oxygenation. However, the influence of different reduced species on carbon isotope enrichment factor for TCE degradation remain unclear.

4. Conclusions

This study aimed to explore the influences of Fe(II) species on TCE degradation and to quantify the carbon isotope enrichment factor during the oxygenation of Fe(II) species. Firstly, Fe(II) species affect TCE degradation through the rate and efficiency of ·OH production as well as the quenching effect. On the one hand, the rate and efficiency of ·OH production were highest for Fe(II)-citrate, followed by Fe(II) adsorbed on Al_2O_3 and mineral structural Fe(II), with the lowest being inorganic $Fe(II)_{dis}$. On the other hand, Fe(II)-citrate had the highest quenching efficiency, followed by inorganic $Fe(II)_{dis}$ and adsorbed Fe(II), with mineral structural Fe(II) having the lowest. Synthetically, the dependence of TCE degradation on different Fe(II) species followed the order: Fe(II) in rNAu-2 > Fe(II)-citrate > $FeCO_3$ > Fe(II) adsorbed on Al_2O_3 > inorganic dissolved Fe(II). Secondly, Fe(II) species had little effect on the carbon isotope enrichment factor for TCE degradation. The carbon isotope

enrichment factors were similar across different Fe(II) systems, but significantly different from those of most other mechanisms.

Conflicts of interest

There are no conflicts to declare.

Data availability

The data used to support the findings of this study are available from the corresponding author upon request.

The SI included 6 Pages, 3 Texts, 3 Figs, and 1 Table. See DOI: https://doi.org/10.1039/d4ra08439j.

Acknowledgements

This work was supported by the National Natural Science Foundation of China (No. 42307095), the Natural Science Foundation of Hubei Province (2022CFB764), the Special Fund of Advantageous and Characteristic disciplines (Group) of Hubei Province, and the Doctoral Fund of Wuhan Business and Technology University (D2022010).

References

1 C. W. Shi, M. Tong, Q. Z. Cai, Z. T. Li, P. Li, Y. X. Lu, Z. X. Cao, H. Liu, H. P. Zhao and S. H. Yuan, Electrokinetic-enhanced bioremediation of trichloroethylene-contaminated low-permeability soils: Mechanistic insight from spatio-temporal variations of indigenous microbial community and biodehalogenation activity, *Environ. Sci. Technol.*, 2023, **57**(12), 5046–5055.

2 C. E. Schaefer, P. Ho, E. Berns and C. Werth, Abiotic dechlorination in the presence of ferrous minerals, *J. Contam. Hydrol.*, 2021, **241**, 103839.

3 J. J. Weatherill, S. Atashgahi, U. Schneidewind, S. Krause, S. Ullah, N. Cassidy and M. O. Rivett, Natural attenuation of chlorinated ethenes in hyporheic zones: A review of key biogeochemical processes and in-situ transformation potential, *Water Res.*, 2018, **128**, 362–382.

4 C. E. Schaefer, P. Ho, E. Berns and C. Werth, Mechanisms for abiotic dechlorination of trichloroethene by ferrous minerals under oxic and anoxic conditions in natural sediments, *Environ. Sci. Technol.*, 2018, **52**(23), 13747–13755.

5 Y. T. He, J. T. Wilson, C. Su and R. T. Wilkin, Review of abiotic degradation of chlorinated solvents by reactive iron minerals in aquifers, *Ground Water Monit R.*, 2015, **35**(3), 57–75.

6 X. X. Liu, S. H. Yuan, M. Tong and D. Liu, Oxidation of trichloroethylene by the hydroxyl radicals produced from oxygenation of reduced nontronite, *Water Res.*, 2017, **113**, 72–79.

7 M. Tong, S. H. Yuan, S. C. Ma, M. Jin, D. Liu, D. Cheng, X. X. Liu, Y. Q. Gan and Y. X. Wang, Production of abundant hydroxyl radicals from oxygenation of subsurface sediments, *Environ. Sci. Technol.*, 2016, **50**(1), 214–221.

8 P. Liao, K. Yu, Y. Lu, P. Wang, Y. Liang and Z. Shi, Extensive dark production of hydroxyl radicals from oxygenation of polluted river sediments, *Chem. Eng. J.*, 2019, **368**, 700–709.

9 N. Chen, Q. Fu, T. Wu, P. Cui, G. Fang, C. Liu, C. Chen, G. Liu, W. Wang, D. Wang, P. Wang and D. Zhou, Active iron phases regulate the abiotic transformation of organic carbon during redox fluctuation cycles of paddy soil, *Environ. Sci. Technol.*, 2021, **55**(20), 14281–14293.

10 A. L. Rose and T. D. Waite, Kinetic model for Fe(II) oxidation in seawater in the absence and presence of natural organic matter, *Environ. Sci. Technol.*, 2002, **36**(3), 433–444.

11 W. Xie, S. Yuan, M. Tong, S. Ma, W. Liao, N. Zhang and C. Chen, Contaminant degradation by ·OH during sediment oxygenation: Dependence on Fe(II) species, *Environ. Sci. Technol.*, 2020, **54**(5), 2975–2984.

12 P. Zhang, J. Liu, H. Yu, D. Cheng, H. Liu and S. Yuan, Kinetic models for hydroxyl radical production and contaminant removal during soil/sediment oxygenation, *Water Res.*, 2023, **240**, 120071.

13 W. J. Xie, P. Zhang, W. J. Liao, M. Tong and S. H. Yuan, Ligand-enhanced electron utilization for trichloroethylene degradation by ·OH during sediment oxygenation, *Environ. Sci. Technol.*, 2021, **55**(10), 7044–7051.

14 H. T. Pham, M. Kitsuneduka, J. Hara, K. Suto and C. Inoue, Trichloroethylene transformation by natural mineral pyrite: The deciding role of oxygen, *Environ. Sci. Technol.*, 2008, **42**(19), 7470–7475.

15 B. Heckel, E. Phillips, E. Edwards, B. Sherwood Lollar, M. Elsner, M. J. Manefield and M. Lee, Reductive dehalogenation of trichloromethane by two different *Dehalobacter restrictus* strains reveal opposing dual element isotope effects, *Environ. Sci. Technol.*, 2019, **53**(5), 2332–2343.

16 C. B. Ottosen, A. M. Murray, M. M. Broholm and P. L. Bjerg, *In situ* quantification of degradation is needed for reliable risk assessments and site-specific monitored natural attenuation, *Environ. Sci. Technol.*, 2019, **53**(1), 1–3.

17 J. Zimmermann, L. J. S. Halloran and D. Hunkeler, Tracking chlorinated contaminants in the subsurface using compound-specific chlorine isotope analysis: A review of principles, current challenges and applications, *Chemosphere*, 2020, **244**, 125476.

18 X. Liang, R. P. Philp and E. C. Butler, Kinetic and isotope analyses of tetrachloroethylene and trichloroethylene degradation by model Fe(II)-bearing minerals, *Chemosphere*, 2009, **75**(1), 63–69.

19 Y. Liu, Y. Zhang, A. Zhou and M. Li, Insights into carbon isotope fractionation on trichloroethene degradation in base activated persulfate process: The role of multiple reactive oxygen species, *Sci. Total Environ.*, 2021, **800**, 149371.

20 P. Zhang, S. H. Yuan and P. Liao, Mechanisms of hydroxyl radical production from abiotic oxidation of pyrite under acidic conditions, *Geochim. Cosmochim. Acta*, 2016, **172**, 444–457.

21 R. Chen, H. Liu, N. Zhang, Y. Huang, X. Y. Deng and M. G. Jin, Flavins enhance the hydroxyl radical production

from $FeCO_3$ oxygenation for organic pollutant degradation, *Chem. Geol.*, 2023, **626**, 121443.

22 W. J. Liao, Z. L. Ye, S. H. Yuan, Q. Z. Cai, M. Tong, A. Qian and D. Cheng, Effect of coexisting Fe(III) (oxyhydr)oxides on Cr(VI) reduction by Fe(II)-bearing clay minerals, *Environ. Sci. Technol.*, 2019, **53**(23), 13767–13775.

23 C. L. Yu, Y. T. Zhang, Y. X. Lu, A. Qian, P. Zhang, Y. P. Cui and S. H. Yuan, Mechanistic insight into humic acid-enhanced hydroxyl radical production from Fe(II)-bearing clay mineral oxygenation, *Environ. Sci. Technol.*, 2021, **55**(19), 13366–13375.

24 B. Ginn, C. Meile, J. Wilmoth, Y. Tang and A. Thompson, Rapid iron reduction rates are stimulated by high-amplitude redox fluctuations in a tropical forest soil, *Environ. Sci. Technol.*, 2017, **51**(6), 3250–3259.

25 H. Yu, P. Zhang, J. Liu, Y. Zheng and N. A. Mustapha, Effects of low-molecular-weight organic acids/thiols on hydroxyl radical production from natural siderite oxidation, *Chem. Geol.*, 2021, **584**, 120537.

26 Y. Liu, A. Zhou, Y. Gan and X. Li, Variability in carbon isotope fractionation of trichloroethene during degradation by persulfate activated with zero-valent iron: Effects of inorganic anions, *Sci. Total Environ.*, 2016, **548–549**, 1–5.

27 A. N. Pham and T. D. Waite, Oxygenation of Fe(II) in natural waters revisited: Kinetic modeling approaches, rate constant estimation and the importance of various reaction pathways, *Geochim. Cosmochim. Acta*, 2008, **72**(15), 3616–3630.

28 N. Chen, M. Geng, D. Huang, M. Tan, Z. Li, G. Liu, C. Zhu, G. Fang and D. Zhou, Hydroxyl radical formation during oxygen-mediated oxidation of ferrous iron on mineral surface: Dependence on mineral identity, *J. Hazard. Mater.*, 2022, **434**, 128861.

29 P. Zhang and S. Yuan, Production of hydroxyl radicals from abiotic oxidation of pyrite by oxygen under circumneutral conditions in the presence of low-molecular-weight organic acids, *Geochim. Cosmochim. Acta*, 2017, **218**, 153–166.

30 C. K. Remucal and D. L. Sedlak, The role of iron coordination in the production of reactive oxidants from ferrous iron oxidation by oxygen and hydrogen peroxide, in *Aquatic Redox Chemistry*, ACS Publications, 2011, pp. 177–197.

31 C. J. Miller, A. L. Rose and T. D. Waite, Importance of iron complexation for Fenton-mediated hydroxyl radical production at circumneutral pH, *Front. Mar. Sci.*, 2016, **3**, 134.

32 K. Rusevova Crincoli and S. G. Huling, Hydroxyl radical scavenging by solid mineral surfaces in oxidative treatment systems: Rate constants and implications, *Water Res.*, 2020, **169**, 115240.

33 A. Gafni, C. Lihl, F. Gelman, M. Elsner and A. Bernstein, $\delta^{13}C$ and $\delta^{37}Cl$ isotope fractionation to characterize aerobic *vs.* anaerobic degradation of trichloroethylene, *Environ. Sci. Technol. Lett.*, 2018, **5**(4), 202–208.

34 Y. Liu, A. Zhou, Y. Gan and X. Li, Roles of hydroxyl and sulfate radicals in degradation of trichloroethene by persulfate activated with Fe^{2+} and zero-valent iron: Insights from carbon isotope fractionation, *J. Hazard. Mater.*, 2018, **344**, 98–103.

35 T. B. Hofstetter, R. P. Schwarzenbach and S. M. Bernasconi, Assessing transformation processes of organic compounds using stable isotope fractionation, *Environ. Sci. Technol.*, 2008, **42**(21), 7737–7743.

36 C. Li, Y. Zhang, Y. S. Zheng, C. W. Shi, Y. X. Lu, Y. T. Zhang and S. H. Yuan, Contaminant transformation during sediment oxygenation: Temporal variation of oxidation mechanisms mediated by hydroxyl radicals and aerobic microbes, *Sci. Total Environ.*, 2024, **919**, 170855.

37 N. Zhang, Y. Liu, Z. Wan, Y. Zhang, W. Xie, P. Zhang, M. Tong and S. Yuan, Dependence of biotic and abiotic H_2O_2 and $^{\bullet}OH$ production on the redox conditions and compositions of sediment during oxygenation, *Environ. Sci. Technol.*, 2024, **58**(8), 3849–3857.

38 J. A. C. Barth, G. Slater, C. Schuth, M. Bill, A. Downey, M. Larkin and R. M. Kalin, Carbon isotope fractionation during aerobic biodegradation of trichloroethene by *Burkholderia cepacia* G4: a tool to map degradation mechanisms, *Appl. Environ. Microbiol.*, 2002, **68**(4), 1728–1734.

39 K. H. Chu, S. Mahendra, D. L. Song, M. E. Conrad and L. Alvarez-Cohen, Stable carbon isotope fractionation during aerobic biodegradation of chlorinated ethenes, *Environ. Sci. Technol.*, 2004, **38**(11), 3126–3130.

40 C. Lihl, L. M. Douglas, S. Franke, A. Pérez-de-Mora, A. H. Meyer, M. Daubmeier, E. A. Edwards, I. Nijenhuis, B. Sherwood Lollar and M. Elsner, Mechanistic dichotomy in bacterial trichloroethene dechlorination revealed by carbon and chlorine isotope effects, *Environ. Sci. Technol.*, 2019, **53**(8), 4245–4254.

41 X. Liang, Y. Dong, T. Kuder, L. R. Krumholz, R. P. Philp and E. C. Butler, Distinguishing abiotic and biotic transformation of tetrachloroethylene and trichloroethylene by stable carbon isotope fractionation, *Environ. Sci. Technol.*, 2007, **41**(20), 7094–7100.

42 J. Huang, A. Jones, T. D. Waite, Y. Chen, X. Huang, K. M. Rosso, A. Kappler, M. Mansor, P. G. Tratnyek and H. Zhang, Fe(II) redox chemistry in the environment, *Chem. Rev.*, 2021, **121**(13), 8161–8233.